Ionic Strength Modulates Excision of Uracil by SMUG1 from Nucleosome Core Particles

Katelyn L. Rioux and Sarah Delaney*

Department of Chemistry, Brown University, Providence, RI, USA

*Correspondence to: Department of Chemistry, Brown University, Providence, RI, USA. Email address: Sarah_Delaney@brown.edu (S. Delaney)

Keywords: Nucleosome core particle; Base excision repair; Single- strand selective monofunctional uracil DNA glycosylase; Ionic strength

Graphical abstract

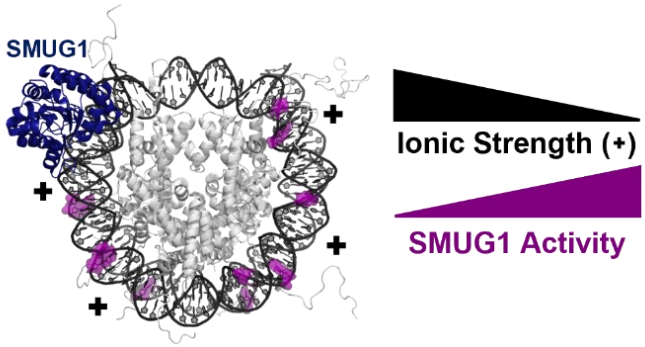

Highlights

- Ionic strength modulates glycosylase activity in nucleosome core particles
- Greater excision of uracil by SMUG1 is observed in lower ionic strength conditions
- Changes in SMUG1 activity likely due to alterations in nucleosome core particle structure and dynamics

ABSTRACT

Ionic strength affects many cellular processes including the packaging of genetic material in eukaryotes. For example, chromatin fibers are compacted in high ionic strength environments as are the minimal unit of packaging in chromatin, nucleosome core particles (NCPs). Furthermore, ionic strength is known to modulate several aspects of NCP dynamics including transient unwrapping of DNA from the histone protein core, nucleosome gaping, and intra- and internucleosomal interactions of the N-terminal histone tails. Changes in NCP structure may also impact interactions of transcriptional, repair, and other cellular machinery with nucleosomal DNA. One repair process, base excision repair (BER), is impacted by NCP structure and may be further influenced by changes in ionic strength. Here we examine the effects of ionic strength on the initiation of BER using biochemical assays. Using a population of NCPs containing uracil (U) at dozens of geometric locations, excision of U by single-strand selective monofunctional uracil DNA glycosylase (SMUG1) is assessed at higher and lower ionic strengths. SMUG1 has increased excision activity in the lower ionic strength conditions. On duplex DNA, however, SMUG1 activity is largely unaffected by ionic strength except at short incubation times, suggesting that changes in SMUG1 activity are likely due to alterations in NCP structure and dynamics. These results allow us to further understand the cellular role of SMUG1 in a changing ionic environment and broadly contribute to the understanding of BER on chromatin and genomic stability.

Abbreviations

AAG, Alkyladenine DNA glycosylase; APE1, AP endonuclease 1; bp, base pair; BER, base excision repair; DTT, dithiothreitol; DUP, duplex DNA; HRF, hydroxyl radical footprinting; hUNG, human uracil DNA glycosylase; NCP, nucleosome core particle; PAGE, polyacrylamide gel electrophoresis; PCI, phenol chloroform isoamyl alcohol; PTM, post-translational modification; rDNA, ribosomal DNA; SAFA, semi-automated footprinting analysis; SE, standard error; SHL, super helical location; smFRET, single-molecule fluorescence resonance energy transfer; SMUG1, single-strand selective monofunctional uracil DNA glycosylase; TDG, thymine DNA glycosylase; U, uracil; UDG, uracil DNA glycosylase

1. Introduction

The ionic environment of the eukaryotic cell is dynamic and can broadly affect cellular processes. Fluctuations in ionic strength can arise from extracellular factors and intracellular events that can influence interactions between cellular components [1,2]. Ionic strength affects protein structure and function [3,4], including protein aggregation [5], and nucleic acid binding [6]. Pockets of liquid-liquid phase separation within the nucleus [7,8] also contribute to the dynamic nature of the cell's ionic environment. Genetic material of eukaryotic cells is highly packaged into chromatin within these nuclear regions of changing ionic strength, which may impact how transcriptional, repair, and other cellular machinery interacts with DNA.

Chromatin fibers consist of DNA packaging units known as nucleosome core particles (NCPs) and are compacted in high ionic strength environments [9-12]. An NCP is comprised of ~145 base pairs (bp) of DNA wrapped around two copies each of the histone proteins H2A, H2B, H3, and H4, with a central axis of pseudo-symmetry referred to as the dyad axis (Figure 1) [13]. The overall stability of the NCP is in part driven by interactions between positively charged histone proteins as well as between histones and the negatively charged backbone of DNA. Such electrostatic interactions are sensitive to changes in ionic strength to maintain a balance between histone core integrity and NCP stability [14,15]. The NCP is a dynamic structure that can undergo unwrapping of DNA in the entry/exit regions [16], compaction and gaping of the NCP gyres [10,17], and association of histone N-terminal tails with the nucleosomal DNA [18-20], all of which are influenced by ionic strength. Histone octamers are also subjected to post-translational modifications (PTMs), exchange of histones for variant versions, as well as interactions with histone chaperones and chromatin remodelers that contribute the dynamic nature of NCPs [21-23].

DNA repair is impacted by the packaging of DNA into NCPs, which poses a significant barrier to the repair machinery. In this work we focus on initiation of the base excision repair (BER) pathway. The initiation is catalyzed by a glycosylase, which excises a modified nucleobase from the sugar-phosphate backbone. Using NCPs, biochemical experiments have shown that glycosylase activity is modulated by the rotational and translational positioning of DNA [24-37]. Typically, glycosylases can more easily access lesions that face outward towards solution compared to those that face inward towards the histone protein core. Additionally, lesions in the entry/exit region of NCPs are more accessible to glycosylases due to transient and spontaneous unwrapping of the DNA from the histones [25,28,31-34,38,39]. Notably, these results of biochemical experiments are consistent with *in vivo* genome-wide mutation mapping [40].

Single-strand selective monofunctional uracil DNA glycosylase (SMUG1) is one of eleven known human glycosylases [41,42]. SMUG1 has a wide substrate range, including uracil (U), and can excise lesions from both single- and double-stranded DNA [42,43]. SMUG1 uses an intercalating "helical wedge" that distorts DNA to access and repair a lesion [44]. SMUG1 has been shown to excise U from U:G [39,45,46] and U:A [47] bp in NCPs, although in many locations of the NCP its activity is significantly diminished compared to duplex DNA.

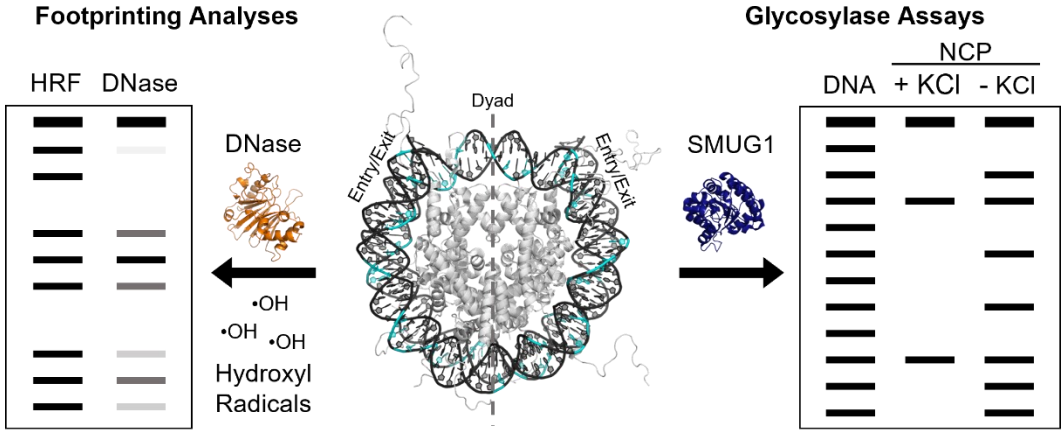

Figure 1. General workflow of SMUG1 activity assessment on NCPs. NCP cartoon (center) was created by merging PDB: 3lz0 (an NCP containing Widom 601 DNA) with PDB: 1kx5 (an NCP

containing histones with intact N-terminal tails). Global C to U substitutions on the "I strand" of 601 DNA are highlighted in cyan and the dyad axis and entry/exit region are indicated. Schematic representation of PAGE analysis of footprinting by HRF and DNase is shown on the left. Schematic representation of PAGE analysis of SMUG1 activity on duplex and NCPs in higher and lower ionic strength conditions is shown on the right.

Here we use an *in vitro* NCP model system to determine the effects of ionic strength on the excision of U by SMUG1 (Figure 1). The U:G bp represents deamination of cytosine in a C:G bp and was chosen as a prototypic damage type for BER. Ranges of ionic strength were chosen in the context of reported cellular concentrations of various ions, and in particular K^+ which can reach 150 mM [48-53]. Total physiological ionic strength concentrations of monovalent cations have been reported to reach ~100-200 mM, with fluctuations surrounding compartments of the nucleus [48-53]. We employ complementary footprinting techniques using hydroxyl radicals and DNase to assess the NCP structure. SMUG1 reactions were performed on U-containing duplex and NCPs in different ionic strength environments. We find that SMUG1 activity on NCPs is modulated by ionic strength and that lesion excision is better at lower ionic strength, likely due to NCP structure and/or dynamics.

2. Materials and Methods

2.1 Oligonucleotide synthesis and purification

All DNA was synthesized using phosphoramidite chemistry on a MerMade4 (BioAutomation) DNA synthesizer. Phosphoramidites were purchased from Glen Research. All duplex controls and NCP samples used the 145-mer Widom 601 sequence (Scheme S1) [54]. Nucleobases of the "I strand" are numbered as 1 to 145 (from the 5′- to 3′-end) with each complementary nucleobase on the "J strand" indicated by the corresponding negative number.

U damage was globally incorporated to form lesion DNA strands (601 I or 601 J strand) using previously reported methods [25]. The Poisson distribution (λ=0.355) was used to determine the molar ratio used to create a C/U mixture to ensure that 95% of DNA contained, at most, one U per strand. U-containing (I or J strand) and non-lesion DNA (I strand) were synthesized with the 5′-trityl group removed and purified by 8% denaturing polyacrylamide gel electrophoresis (PAGE).

The non-lesion containing J strand was prepared via ligation of shorter component strands using T4 ligase (New England Biolabs) and scaffold DNA strands (Scheme S2). This method was used only for the non-lesion J strand for optimal product yield. Component and scaffold strands were synthesized with the 5′-trityl group retained for reverse-phase HPLC purification (Dynamax Microscorb C18 column, 250 x 10 mm; A = acetonitrile [MeCN], B = 30 mM NH_4OAc; 5:95-35:65 A:B over 30 min at 3.5 mL/min). The trityl group was removed via incubation in 20% v/v aqueous glacial acetic acid for 1 h at ambient temperature, followed by a second round of HPLC purification at 90 °C (Agilent PLRP-S column, 250 x 4.6 mm; A = 100 mM triethylammonium acetate [TEAA] in 5% aqueous MeCN, B = 100 mM TEAA in MeCN; 0:100-15:85 A:B over 35 min then 15:85-35:65 A:B over 5 min at 1 mL/min). Electrospray ionization mass spectrometry was used to confirm the identity of component and scaffold strands. The ligated non-lesion J strand was purified by 8% denaturing PAGE.

Three single-stranded internal standard DNA sequences were designed such that they would not co-migrate with any U cleavage product (32-mer, 40-mer, and 98-mer) (Scheme S1). The 32-mer and 98-mer standards were used for normalization and loading controls for the U-containing I strand. The 40-mer and 98-mer standards were used for normalization and loading

controls for the U-containing J strand. These standards were synthesized with the 5′-trityl group removed and purified by 12%, 10%, and 8% denaturing PAGE, respectively.

2.2 Histone preparation and NCP reconstitution

Canonical *X. laevis* histones (H2A, H2B, H3, H4) were recombinantly expressed and purified according to published protocols [55]. Individual histones were combined in an equimolar ratio and assembled into a histone octamer via salt-gradient dialysis, then purified via size-exclusion [55]. NCPs were reconstituted via salt-gradient dialysis as previously described [55,56]. U-containing DNA was 5′-^{32}P-radiolabeled and annealed to its non-lesion containing complement in annealing buffer (10 mM Tris [pH 8], 50 mM NaCl, 1 mM EDTA). 1 μM duplex DNA and 2 μM octamer were combined in 1:1.07 and 1:1.15 DNA:octamer molar ratio for U-containing I strand and J strand substrate, respectively, in a Slide-a-Lyzer dialysis device (0.1 mL capacity, 3.5 kDa MWCO; Thermo Fisher Scientific). Samples were incubated at 4° C in 2 M NaCl, 10 mM Tris-HCl (pH 7.5), 1 mM EDTA, 1 mM dithiothreitol (DTT) and 0.5 mg/mL BSA. NaCl concentration was reduced stepwise at 1 h intervals (1.2, 1.0, 0.6 M) and 3 h interval (0 M) via dialysis. NCPs were then filtered by centrifugation using a Spin-X Centrifuge Tube filter (0.22 μm, Corning Incorporated) to remove precipitates. Samples were evaluated by 7% native PAGE (19:1 acrylamide:bisacrylamide, 4 °C, 2.5 h, 155 V, 0.25X TBE) and only NCPs with less than 5% duplex DNA were used for subsequent experiments.

2.3 Hydroxyl radical footprinting (HRF)

HRF reactions were performed on NCP samples, based on previously published methods [57,58], to determine solution accessibility at each nucleobase position. Briefly, 7.5 μL of each 10 mM Fe(II)-EDTA, 10 mM sodium ascorbate, and 0.12% w/v aqueous hydrogen peroxide were combined and immediately added to 5 pmol of NCP in 52.5 μL reaction buffer (10 mM Tris-HCl

[pH 7.5], 1 mM EDTA). The reaction was incubated in the dark at ambient temperature for 8 min and quenched with 16 µL 50 mM EDTA in 25% v/v glycerol. NCPs were immediately run on a 7% native PAGE to separate NCPs from any duplex DNA that may have disassociated during the reaction. The NCP band was excised from the gel and eluted into buffer (0.3 M NaOAc, 1 mM Tris-HCl [pH 8.0], 1 mM EDTA) overnight at 37° C and 60 rpm shaking. Eluent was concentrated and extracted from proteins using 25:24:1 phenol:chloroform:isoamyl alcohol (PCI). DNA fragments in the resulting aqueous phase were desalted via ethanol precipitation by addition of 30 µL co-precipitation agent (0.3 M NaOAc, 1 mM EDTA, 0.5 mg/mL tRNA) and 600 µL ethanol and incubation on dry ice for at least 30 min, followed by centrifugation. Pelleted DNA was resuspended in 50% v/v formamide and loaded alongside Maxam-Gilbert A/G sequencing ladders onto a 10% denaturing PAGE. The sample was split in two and half the sample was run for 1.5 h to resolve bands 15-80 and the other half was run for 3 h to resolve bands 81-136. Gels were imaged by phosphorimagery and bands were quantified using semi-automated footprinting analysis (SAFA) software [59]. Each nucleobase position was normalized by dividing the HRF value at a given position by the highest HRF reactivity within that helical turn. Positions with a ratio greater than 0.8, between 0.8 and 0.2, and below 0.2 were assigned as sites that have high, intermediate, and low solution accessibility, respectively.

2.4 DNase digestion

2.5 pmol of duplex DNA and NCPs were treated with 0.02 or 0.002 units of DNase I (New England Biolabs) in 25 µL total reaction volume (10 mM Tris-HCl [pH 7.6], 2.5 mM $MgCl_2$, 0.5 mM $CaCl_2$) for 5 min at 37 °C. Duplex samples were quenched with the addition of 12.5 µL of 100 mM EDTA and 1 mg/mL calf-thymus DNA. NCP samples were quenched with 8.3 µL of 50 mM EDTA, 0.5% SDS, 0.2 mg/mL proteinase K (Thermo Fisher Scientific), then incubated for 2

h at 50 °C and extracted twice against PCI. All samples were desalted via ethanol precipitation. Samples were loaded with Maxam-Gilbert A/G sequencing ladders onto a 10% denaturing PAGE for 1.5 h to visualize cleavage of duplex DNA and nucleosomal DNA from DNase digestion.

2.5 Global assessment of SMUG1 activity

Human SMUG1 was obtained from New England Biolabs and the total concentration was determined by Bradford assay using γ-globulin standards (Bio-Rad Laboratories). To assess glycosylase activity on U-containing duplex DNA as a function of time, 0.5 pmol duplex 601 I strand DNA was mixed with 10 pmol SMUG1 in 20 µL total reaction volume. The reaction buffer contained 20 mM Tris-HCl (pH 7.6), 50 mM NaCl, +/-150 mM KCl, 1 mM EDTA, 1 mM DTT, and 0.2 mg/mL BSA. Conditions in the presence of 150 mM KCl were termed HIGH salt conditions while without 150 mM KCl were termed LOW salt conditions. Samples were incubated for 1, 5, 10, 30, or 60 min at 37 °C. A negative control sample (-E) was incubated for 60 min with no enzyme present to reveal any pre-existing damage or incidental damage of the substrate before and during the reaction. All samples were quenched with equal volume (20 µL) of 1 M NaOH for 2 min at 90 °C. The quench solution included the 5′-^{32}P-radiolabaled internal standards. Samples were then desalted by ethanol precipitation, resuspended in 50% v/v formamide, and split in half. Half the sample was loaded onto a 10% denaturing PAGE to resolve bands 16-74 and the other half loaded onto an 8% gel to resolve bands 75-124. Gels were imaged by phosphorimagery and band intensities were quantified by SAFA software.

To assess glycosylase activity on NCPs, 0.5 pmol of U-containing NCPs were mixed with 10 pmol SMUG1 in 20 µL total reaction volume of four possible reaction buffers. Tris buffers contained 20 mM Tris-HCl (pH 7.6), 50 mM NaCl, +/-150 mM KCl, 1 mM EDTA, 1 mM DTT, and 0.2 mg/mL BSA. HEPES buffers contained 50 mM HEPES (pH 7.6), 50 mM NaCl, +/-150

mM KCl, 1 mM EDTA, 1 mM DTT, and 0.2 mg/mL BSA. Samples were incubated for 60 min at 37 °C, including a negative control sample (-E) with no enzyme present to reveal any pre-existing damage or incidental damage of the substrate before and during the reaction. All samples were quenched with equal volume (20 µL) of 1 M NaOH for 2 min at 90 °C. The quench solution included the 5′-^{32}P-radiolabaled internal standards. DNA fragments were then extracted from proteins using PCI. No significant detection of radioactivity in the organic phase of PCI extraction signifies that stable DNA-histone crosslinks are not forming under these experimental conditions. Samples were then desalted by ethanol precipitation, resuspended in 50% v/v formamide, and split in half. Half the sample was loaded onto a 10% denaturing PAGE to resolve bands 16-74 and the other half loaded onto an 8% gel to resolve bands 75-124. Gels were imaged by phosphorimagery and band intensities were quantified by SAFA software.

Intensities of the internal standards (32-mer for I strand 10% gel, 40-mer for J strand 10 % gel, 98-mer for 8% gels) were used as loading control references to normalize band intensities in each lane. Negative controls (-E) were subtracted from glycosylase treated samples. For duplex DNA excision (DUP), the standard error (SE) of DUP was calculated by $SE = \sigma/\sqrt{n}$ where σ is the standard deviation and n is sample size (n=3). A two-tailed Welch's t test ($\alpha = 0.05$) was performed to obtain the p value at every U site for each DUP reacted in LOW conditions (DUP_{LOW}) in comparison to in HIGH conditions (DUP_{HIGH}). All statistical analyses were conducted using R. We considered $p < 0.05$ to be significant. A ratio of corrected band intensity for DUP_{LOW} to DUP_{HIGH} was determined and the following equation was used to propagate error.

$$\left(\frac{\Delta A}{A}\right)^2 = \left(\frac{\Delta B}{B}\right)^2 + \left(\frac{\Delta C}{C}\right)^2$$

A is the newly created DUP_{LOW} /DUP_{HIGH} ratio and ΔA is the associated SE. ΔA is calculated using the SE and values of DUP_{LOW} (B) and DUP_{HIGH} (C). For NCP assays, at each U site, a ratio of

corrected band intensity for NCPs to duplex DNA (NCP/DUP) was determined and SE was calculated (n=3). A two-tailed Welch's t test ($\alpha = 0.05$) was performed to obtain the p value at each U site for each NCP/DUP reacted in LOW conditions in comparison to in HIGH conditions. We considered $p < 0.05$ to be significant.

3. Results

3.1 Assembly and characterization of NCP population containing globally incorporated uracil

In this work, the NCP model system utilized the Widom 601 strong positioning sequence [60]. The use of a positioning sequence ensures a homogeneous population of NCPs with the DNA reproducibly bound to the histone core. The two complementary strands of 601 DNA are designated the I strand and J strand based on nomenclature used in the X-ray crystal structure of 601 NCPs [54]. We numbered the nucleobases of the I strand as 1 to 145 (from the 5′- to 3′-end) with each complementary nucleobase on the J strand indicated by the corresponding negative number.

The 601 sequence was chemically synthesized to include U as a prototypic modified nucleobase repaired by the BER pathway. U was incorporated into one strand of the 601 DNA using a statistical distribution that ensures no more than one U per strand. The lesion can be incorporated at any one of the 46 or 34 cytosine positions in the I or J strand, respectively, using the Poisson distribution. The global U-containing DNA was then used to assemble NCPs, formation of which was confirmed by native PAGE (Figure 2). Single-stranded and duplex DNA migrate faster than the NCPs. This population of NCPs contains U in a variety of geometric positions (*vide infra*) and was used in our repair fingerprint assay [25] to determine excision activity of SMUG1 under varying conditions of ionic strength. Glycosylase assays were performed

using the buffers [20 mM Tris (pH 7.6), 50 mM NaCl, 1 mM EDTA, 1 mM DTT, 0.2 mg/mL BSA] or [50 mM HEPES (pH 7.6), 50 mM NaCl, 1 mM EDTA, 1 mM DTT, 0.2 mg/mL BSA]. These buffers either contained or lacked 150 mM KCl. The conditions lacking KCl are referred to as low salt (LOW) and those including 150 mM KCl are referred to as high salt (HIGH). This range of ionic strength encompasses reported physiological conditions and microenvironments of the cell where SMUG1 may encounter U [50-53,61].

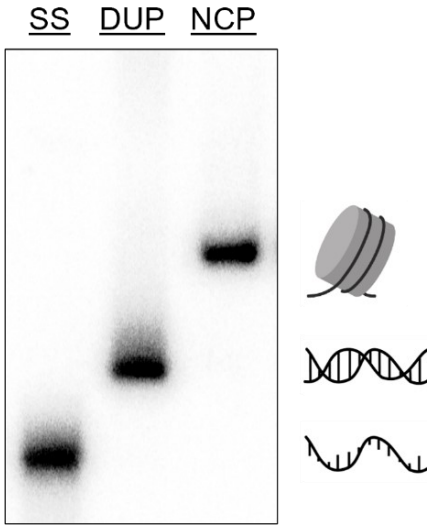

Figure 2. Representative native PAGE characterization of NCP assembly. The NCPs (NCP) migrate slower relative to duplex (DUP) and single-strand (SS) controls. All substrates contain globally-incorporated U.

3.2 Rotational positioning of nucleosomal DNA

Rotational positioning of the nucleosomal DNA was characterized using hydroxyl radical footprinting (HRF; Figure 3A) and DNase footprinting (Figure 3B), as described previously [24,46]. HRF and DNase footprinting are complementary techniques that use chemical and enzymatic reagents, respectively, to map each nucleobase's orientation relative to the histone core. A nucleobase can face outwards towards solution (OUT), inwards towards the histones (IN), or in between these two (MID) (Figure 3C). HRF provides information about rotational positioning

based on solution accessibility of the DNA to the hydroxyl radical (17 Da) while the DNase enzyme (31,000 Da) is a larger footprinting reagent. These experiments were conducted using conditions compatible with the footprinting reagents and their chemical reactivity (see the materials and methods) and establish baseline structural information regarding rotational positioning of DNA in the NCPs.

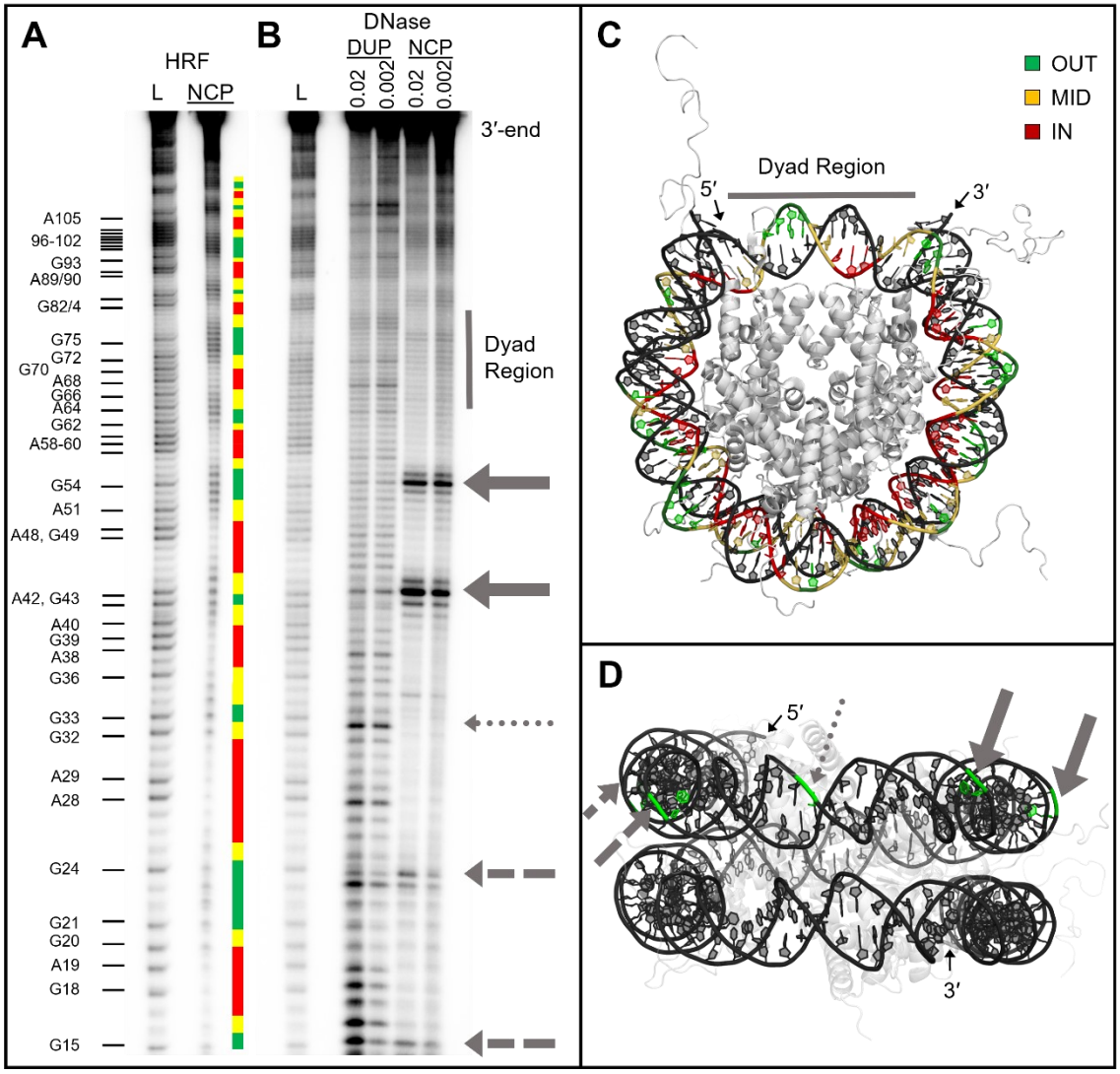

Figure 3. Rotational positioning of nucleobases in the I strand of the NCP as determined by HRF and DNase footprinting. (A) Representative denaturing PAGE of HRF for the NCP (NCP) and an A/G Maxam/Gilbert sequencing ladder (L). Color-coded bar depicts OUT (green), MID (yellow) and IN (red) nucleobases. (B) Representative denaturing PAGE of DNase footprinting of 601 duplex DNA control (DUP), NCP (NCP), and A/G Maxam/Gilbert sequencing ladder (L). Each substrate was reacted with 0.02 U or 0.002 U of DNase. (C) Top-down view of NCP with rotational

positioning determined by HRF indicated as OUT (green), MID (yellow), and IN (red). Complementary J strand is in black and dyad region is indicated. (D) Side view of NCP with rotational positioning determined by DNase. From left to right, arrows indicate positions 55, 44, 34, 25, and 16. Thick solid, dashed, and thin dotted arrows represent decreasing amounts of cleavage by DNase, respectively.

To create an HRF profile, Fenton chemistry generates hydroxyl radicals, which subsequently cleave the DNA backbone in regions not bound to histone proteins [57,58]. This footprinting technique creates an oscillating pattern of cleavage that describes rotational positioning. Dark bands represent sites that are susceptible to hydroxyl radicals and therefore are solution accessible (Figure 3A). Bands were quantified and normalized within each helical turn where a value of 1 represents maximal solution accessibility (Table S1). We defined values greater than 0.8 (OUT, green), between 0.2 and 0.8 (MID, yellow), less than 0.2 (IN, red) and are indicated in the color-coded bar in Figure 3A. The rotational positioning determined by HRF was also mapped onto an NCP (Figure 3C). These levels of solution accessibility are consistent with the rotational positions observed in the X-ray crystal structure of the 601 NCP [54].

As a complementary footprinting reagent, DNase is much larger in size than hydroxyl radical and provides additional context to understand how SMUG1 interacts with the NCP. Similar to the HRF profile, dark bands represent cleavage at nucleobases that are accessible by DNase (Figure 3B). The most outward facing positions are observed every ~10 base pairs with the extent of cleavage by DNase indicated by the arrow pattern. Notably, some OUT positions are not cleaved efficiently by DNase (Figure 3D). For instance, the dyad region shows little to no cleavage by DNase (Figure 3B, gray bracket). DNA in the dyad region may be inaccessible for binding and/or enzymatic activity by DNase because it is underwound [58,62] and/or is less dynamic than other regions of the NCP [16,38,63,64].

Taken together, the HRF and DNase footprinting demonstrate the rotational positioning of DNA in the NCP and reflect nuances in the solution accessibility of nucleosomal DNA. SMUG1 glycosylase activity was interpreted in the context of this footprinting information.

3.4 Assessment of SMUG1 activity on duplex DNA

Prior to examining SMUG1 activity on NCPs, it is important to understand the extent to which ionic strength affects excision of U from duplex DNA that is not bound to histones. Therefore, SMUG1 excision activity on duplex 601 DNA was assessed in Tris buffer in the presence or absence of 150 mM KCl as a function of time. For each U site, normalized excision values were plotted as a ratio of excision in LOW conditions (DUP_{LOW}) relative to HIGH conditions (DUP_{HIGH}) (Figure 4; Figure S1). A ratio of 1 indicates comparable SMUG1 excision activity in LOW and HIGH conditions, which is the observation at 10 min and longer for all U sites. But at most U sites at 1 min, and some U sites at 5 min, SMUG1 has greater excision activity in LOW conditions than in HIGH. In other words, SMUG1 does not excise U as efficiently in HIGH conditions as in LOW until after 5 min. Similar experiments using duplex DNA in HEPES buffer were conducted at 60 min resulting in comparable SMUG1 excision activity in LOW and HIGH conditions (Figure S2). These duplex experiments provide a baseline understanding of how SMUG1 interacts with 145-mer U-containing duplex DNA over time under these different conditions and serve as a comparison point to SMUG1 activity on NCPs.

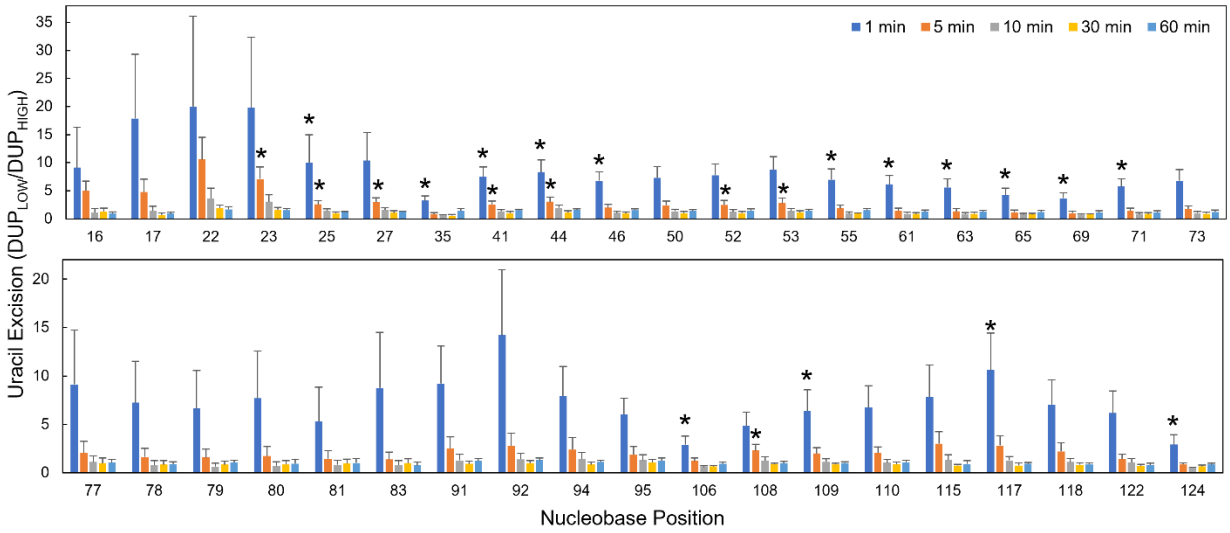

Figure 4. Excision of U by SMUG1 from duplex DNA in HIGH and LOW conditions as a function of time. U excision is plotted as a ratio of excision from duplex in LOW conditions to HIGH conditions, and against nucleobase position. A value of 1 reflects SMUG1 excision activity that is the same on duplex in LOW and HIGH conditions. Error bars represent standard error (n=3). Asterisks denote statistically significant differences between the excision value in LOW conditions and in HIGH conditions ($p < 0.05$). SMUG1 was incubated with the duplex substrate for 1 (dark blue), 5 (orange), 10 (gray), 30 (yellow), or 60 (light blue) min.

3.5 Ionic strength modulates SMUG1 activity on NCPs

SMUG1 activity on the I strand of DNA in NCPs in the Tris buffer system was evaluated next. Due to technical limitations in preparing substantial amounts of lesion-containing NCPs, a time course was not performed. A 60 min incubation with SMUG1 was conducted. Qualitative analysis of these denaturing PAGE gels reveals differences in activity between HIGH and LOW conditions (Figure 5A and 5B, NCP +E lanes). In the NCP under LOW salt conditions SMUG1 activity is increased relative to HIGH. In the dyad region, however, little SMUG1 activity was observed in either condition.

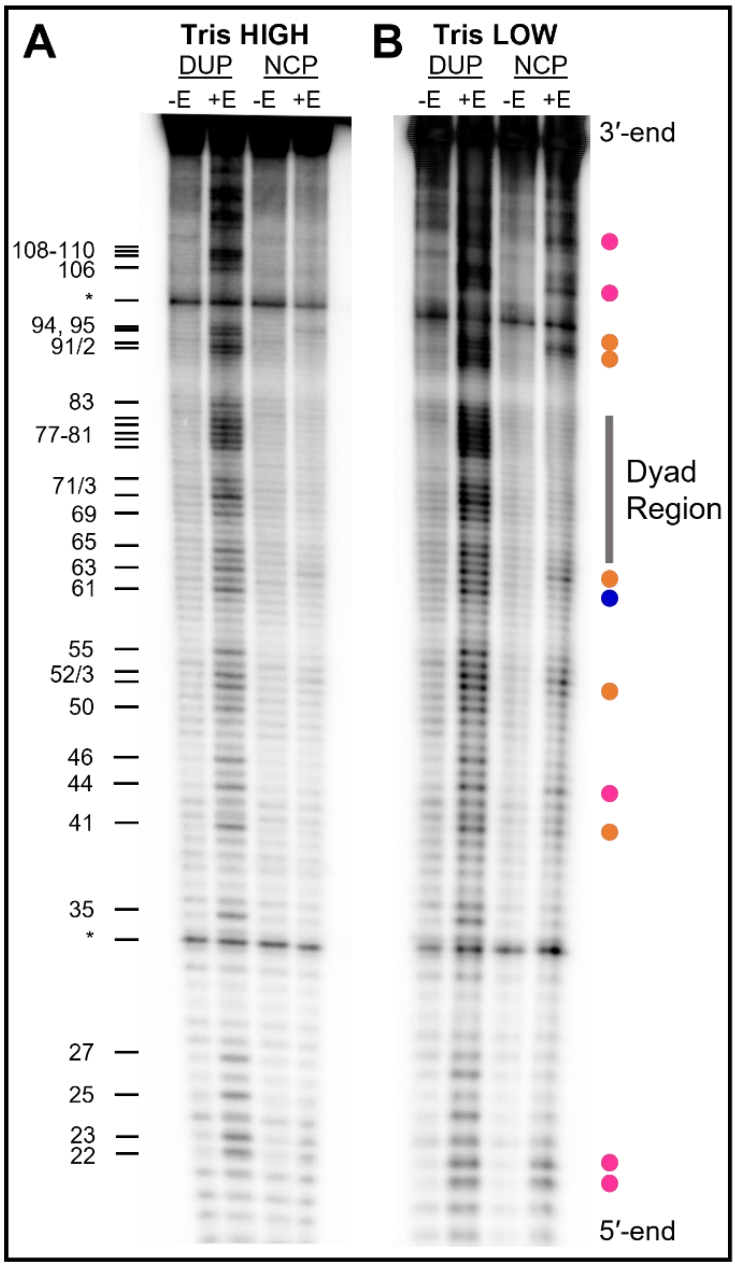

Figure 5. Representative PAGE of U excision by SMUG1 from duplex control (DUP) and NCP substrates (NCP). 601 I strand with global U:G base pairs reacted with SMUG1 (+E). Negative controls (-E), treated with NaOH only to determine any pre-existing or incidental damage from experimental conditions. Internal standards used for normalization are indicated by asterisks. (A) Samples reacted in Tris HIGH conditions. (B) Samples reacted in Tris LOW conditions. Gray bracket indicates dyad region. Color dots denote sites of significantly increased SMUG1 activity between gels categorized by high (pink), intermediate (orange), and low-level changes (blue).

SMUG1 activity was quantitated and plotted versus nucleobase position. The results are presented as a ratio of excision of U from NCP relative to duplex (Figure 6, bar graph). A value of 1 would therefore reflect comparable activity of SMUG1 in NCP and duplex. Relative solution accessibility, as determined by HRF, is also plotted (Figure 6, gray area plot).

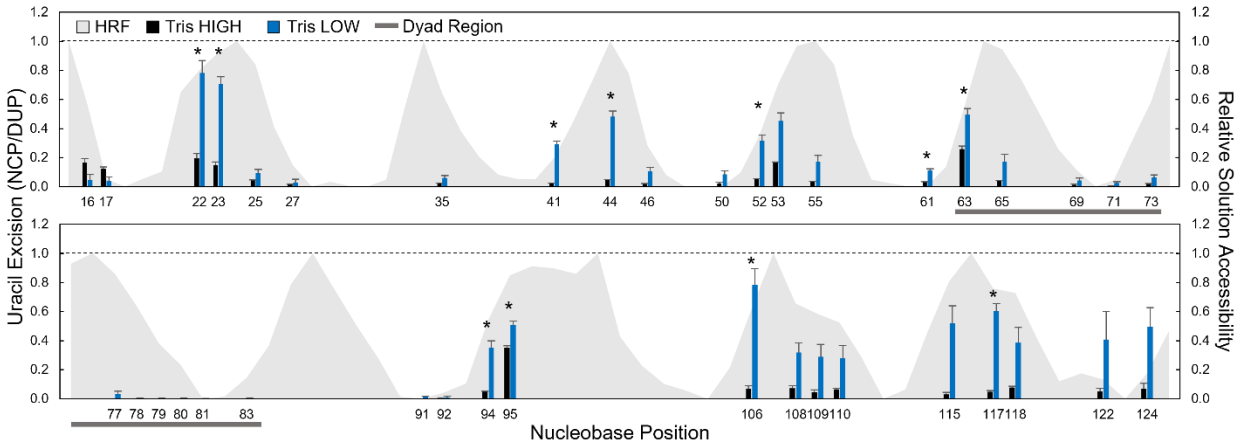

Figure 6. Excision of U by SMUG1 from NCPs (U in the I strand). At each U site, product yield is indicated as the ratio of excision from the NCP relative to duplex (NCP/DUP). A ratio of 1, indicated by the dotted line, represents comparable excision from the NCP and duplex. Nucleobase positions are labeled from the 5'- to 3'-end. Excision by SMUG1 in Tris HIGH conditions (black bars) and in Tris LOW conditions (blue bars). HRF profile (gray area) represents solution accessibility at each nucleobase position. Error bars represent standard error (n=3). Asterisks denote statistically significant differences in U excision ratios between Tris HIGH and Tris LOW at that site ($p < 0.05$).

Each U site was then categorized based on the absolute difference in excision ratio in HIGH and LOW conditions and color coded to indicate the greatest (>0.3, pink dot), intermediate (0.1-0.3, orange dot), and lowest level of change in activity (<0.1, blue dot) (Figure 5). In HIGH conditions, SMUG1 has little to no activity across the NCP, with the exception of sites 63 and 95 (Figure 6, black bars). In contrast, increased SMUG1 activity at various geometric positions in NCPs is observed in LOW conditions (Figure 6, blue bars): sites 22, 23, 41, 44, 52, 61, 63, 94, 95, 106, and 117. Under both LOW and HIGH buffer conditions, lesions in the dyad region are refractory to repair.

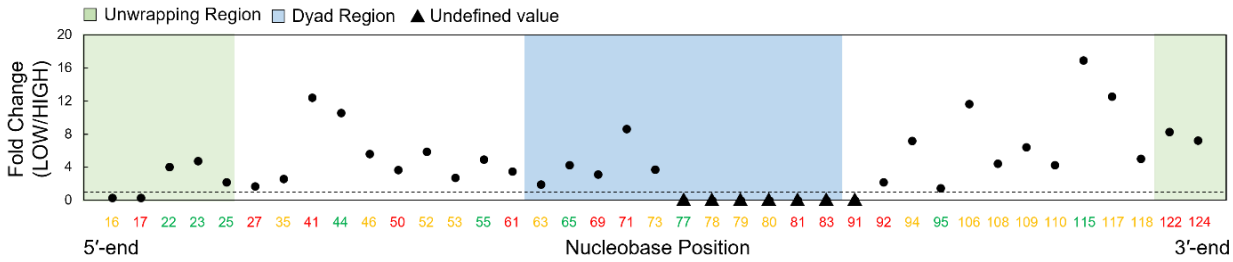

Figure 7. Fold change of SMUG1 excision activity in LOW relative to HIGH conditions. A value greater than 1, indicated by the dotted line, indicates increased activity in LOW conditions compared to HIGH. The numbered nucleobase positions indicate the location of U and are colored based on rotational position as OUT (green), MID (yellow), and IN (red). Translational positions of U are represented by area shading: entry/exit regions (green area) and dyad region (blue area). Positions 77-81, 83, and 91 have undefined fold changes (triangle) because the denominator HIGH excision values are 0.

The fold change in SMUG1 activity for LOW relative to HIGH conditions reveals increased excision ranging from 1.5-17-fold at all sites in the NCP except 16, 17, and 77-91 (Figure 7, Table S2). Fold changes in activity vary with no apparent correlation to rotational positioning. At positions 16 and 17, which are in the 5′-end unwrapping region (Figure 7, green area), fold change is less than 1, indicating greater SMUG1 activity in HIGH conditions compared to LOW.

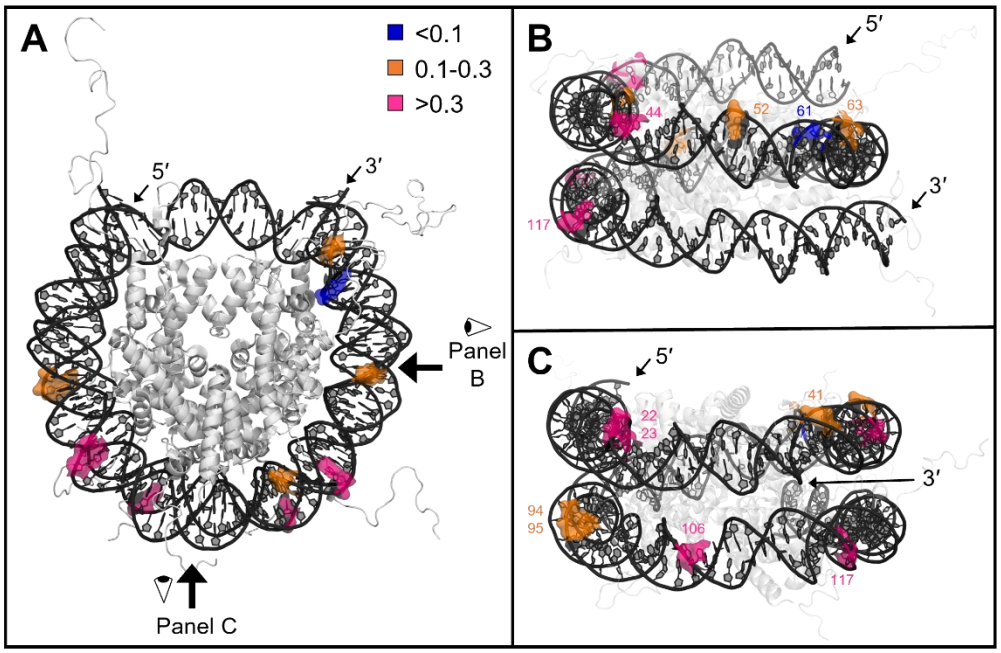

Figure 8. Model of NCP highlighting differences in SMUG1 excision activity between HIGH and LOW Tris buffer conditions. U sites are categorized based on differences in excision ratios of less than 0.1 (blue), 0.1-0.3 (orange), and greater than 0.3 (pink). Only positions at which excision ratios in HIGH and LOW conditions are significantly different ($p<0.05$) are shown. NCP model was generated by merging PDB:1kX5 (octamer core) and PDB:3lz0 (Widom 601 DNA). (A) Top view of NCP. The 5′- and 3′-ends of the I strand are indicated. (B, C) Side views of NCP from the perspectives indicated in (A). Octamer core is transparent for clarity.

Differences in SMUG1 activity levels between LOW and HIGH conditions were mapped onto the NCP (Figure 8). U sites with the greatest level of change are highlighted in pink, while those with intermediate and the lowest level of change are orange and blue, respectively. U sites 41, 44, 52, 61, and 63 cluster in super helical locations (SHL) -1, -2, and -3 (Figure 8A, 8B). On the same gyre, at SHL -5, positions 22 and 23 experience change in SMUG1 activity greater than 0.3 (Figure 8A, 8C). On the opposite gyre at SHL 2, positions 94 and 95 experience intermediate changes in SMUG1 activity. Sites 106 and 117 have high change levels in SHL 3 and 4.5 respectively.

3.6 Ionic strength is the dominant factor modulating SMUG1 activity in other systems

SMUG1 excision activity was also examined in the HEPES buffer system. Similar to Tris, LOW conditions also facilitate SMUG1 activity (Figure S3, purple bars). Fold changes in SMUG1 activity range from 1 to 37-fold (Figure S4, Table S2) and cluster similarly to those in Tris (Figure S5). Comparable experiments were also conducted to examine excision from the J strand of 601 duplex and NCP. Similar to the results observed for the I strand, excision of U by SMUG1 is higher in LOW conditions relative to HIGH (Figure S6). These results obtained using a HEPES buffer and on the J strand provide further support that ionic strength, rather than an artifact of the buffer or a strand-specific parameter (such as sequence context), is modulating SMUG1 activity.

4. Discussion

In this work, we used our repair fingerprinting technique to examine the influence of ionic strength on SMUG1 excision activity in NCPs. We used a range of ionic strength concentrations to capture dynamic nucleosomal DNA interactions that SMUG1 may encounter in the cellular environment. In our previous work with SMUG1, we observed poor activity of SMUG1 on a site-specifically incorporated U:G bp positioned near the dyad region of an NCP [45]. Limited SMUG1 activity was similarly observed for U:G bps globally distributed in NCPs at a variety of geometric positions [39,46]. This previous research featured conditions comparable to the HIGH ionic strength used in the current work. Here we find that SMUG1 activity depends on ionic strength and that lesion excision is more effective at lower ionic strength.

SMUG1 has excision activity on both single- and double-stranded DNA and it is known that the substrate preference for duplex depends on ionic strength [65]. Here we show that when U-containing 601 duplex DNA is the substrate, SMUG1 is inhibited in HIGH conditions at shorter time points (1, 5 min). At 10 min and longer, SMUG1 excision is comparable in both HIGH and LOW conditions. These experiments measure strand cleavage, which reflects both SMUG1 binding and excision chemistry. While these measurements do not directly attribute the difference in activity exclusively to binding or chemistry steps, there is literature evidence demonstrating that binding of some glycosylases is dependent on ionic strength [66-68]. Human uracil DNA glycosylase (hUNG) [66] and alkyladenine DNA glycosylase (AAG) [67] both have decreased binding affinity for short oligonucleotides in high ionic strength (150-200 mM). Glycosylases have also been shown to be less processive in high ionic strength [68,69]. Our results with longer duplex DNA show that higher ionic strength decreases U excision at short incubation times. A potential explanation for this observation is that SMUG1 has decreased binding affinity and/or is slower to

identify the target lesion on a longer oligonucleotide in higher ionic strength conditions. Nevertheless, the similar levels of SMUG1 activity at and beyond 10 min in duplex indicate that any changes observed in NCPs, which utilized a 60 min incubation, are not entirely an inherent property of SMUG1's interactions with duplex DNA.

Next, we considered that the observed changes in SMUG1 activity could be due to changes in NCP dynamics and/or structure that occur with ionic strength, namely unwrapping of DNA in the entry/exit regions, compaction of the NCP gyres, and association of the histone tails. Using a variety of techniques, several prior works examined the influence of salt, ranging from 10-800 mM Na^+ and/or K^+, on NCP structure. At 10 mM salt, the NCP is most often wrapped but its gyres are not compacted [18]. Cryo-EM structures show that in low salt, NCPs adopt more open conformations that resemble nuclear NCPs with less compaction [10]. At concentrations as low as 50 mM salt, single-molecule fluorescence resonance energy transfer (smFRET) experiments determined that the nucleosome experiences slow spontaneous gaping [17]. The gaping of a nucleosome refers to the two gyres separating from each other like the hinged motion of a clam shell. In low salt conditions, repulsion of the negatively charged DNA gyres drives nucleosome gaping [10]. Nucleosome gaping was first thought to only contribute to chromatin compaction in chromatin fibers [12] but has since been shown to occur in mono-nucleosomes [17,22] such as those used in the current work. As salt levels increase (to ~160 mM), the gyres of the NCP are compacted, and the histone tails dissociate. The DNA in the entry/exit regions also experience increased unwrapping, as shown by smFRET [16]. At 600 mM salt, about 50% of the NCP is unwrapped [18]. Then, at very high salt conditions (≥ 800 mM), histone core disassembly occurs with the loss of the H2A/H2B dimer [21]. In our experimental conditions, the NCP in LOW conditions experiences less compaction (more gaping), less unwrapping, and more histone tail

association than in HIGH conditions. Each of these dynamic factors create unique microenvironments for each nucleobase position in the NCP.

Sites with the highest changes in activity between LOW and HIGH conditions (Figure 8, pink), 22, 23, 44, 106, and 117, correlate to changes in NCP dynamics in the low ionic strength environment. All except site 117 reside in the major groove, which may allow for improved access by SMUG1 to flip the lesion and complementary base through the major groove in LOW conditions. They also most closely interact with an H2B tail which, when dissociated from the DNA in HIGH conditions, may interfere with SMUG1 accessibility. Sites 22 and 23 are both OUT sites that face away from the opposite NCP gyre and reside on the edge of the NCP that experiences slow spontaneous gaping in LOW conditions allowing for improved access to repair. NCP dynamics in low ionic strength may also alleviate some increased twist of 22 and 23 from stretching of the DNA in the SHL 5 region. Sites, 44, 106, and 117 are all OUT and MID sites that may experience the full effect of the gaping transition of the nucleosome in LOW conditions based on their locations (Figure 8B, 8C). Together these NCP dynamics experienced in changing ionic strengths have a significant impact on SMUG1 activity.

In high ionic strength environments, the NCP experiences more unwrapping at the DNA entry/exit regions. Increasing amounts of counterions facilitate unwrapping by driving the DNA away from the histone core [16]. Sites 16 and 17 of the 5′-end entry/exit region, do not have increased SMUG1 activity in LOW conditions because the NCP is more wrapped. On the cusp of the unwrapping region, sites 22 and 23 do not experience this same result as sites 16 and 17 due to the local DNA structure and dynamics. The increase in activity in the 3′-end region can be explained by the known increased propensity for this end of the 601 DNA to unwrap from histones

[70]. While the rest of the nucleosome experiences compaction in higher ionic strength, the entry/exit regions may be more accessible to SMUG1 as unwrapping is facilitated.

We and others have shown that glycosylase activity generally correlates with rotational positioning, where OUT sites that are more solution accessible are more likely to be repaired [24-29]. But SMUG1 is unique in that in HIGH conditions it has little to no activity regardless of rotational positioning, with the exception being sites 63 and 95 where the high solution accessibility may help facilitate SMUG1 activity. In LOW conditions, SMUG1 activity does largely correlate with rotational positioning (Figure 6). However, 65 is an OUT site that is not repaired efficiently by SMUG1. DNase similarly displays no cleavage at this outward site indicating that the NCPs in these regions are largely inaccessible to enzymes, possibly due to severe DNA kinking in the SHL -1 region [38,54] or interference from nearby H3 and H4 tails. Position 35 is characterized as MID based on HRF but is less readily excised than other midway sites. DNase also has limited activity at this site. The HRF and DNase footprints demonstrate that each position is uniquely accessible as determined by the specific structural microenvironments of the NCP. It should be noted that HRF and DNase experiments were conducted in low salt conditions suitable for the respective footprinting techniques. It has been previously reported that increasing salt conditions, from 0 to 800 mM NaCl, did not influence the resulting HRF profile on NCPs [71]. DNase activity is limited by salt concentrations higher than 100 mM [72]. These footprinting assays contribute to our baseline understanding of NCP rotational positioning and inherrant structural properties.

Another region of interest is two nearby pairs of adjacent U lesions at sites 91/92 and 94/95. A significant difference in SMUG1 activity is seen at sites 94/95 in HIGH conditions (94 is not readily excised whereas 95 is one of the few sites that is excised in HIGH). In LOW conditions,

intermediate SMUG1 activity is observed at both 94/95. But SMUG1 activity at the nearby pair 91/92 is very low in both LOW and HIGH conditions. Rotational positioning may influence SMUG1 activity because 91/92 are IN positions whereas 94/95 are MID/OUT. In LOW conditions, 91/92 are closer to the hinge of the gaping nucleosome than 94/95 and may not benefit from the more open conformation.

The ionic strengths used in this work were chosen as a range that encompasses reported physiological ionic strength conditions to capture the effects of changing NCP dynamics and/or structure on repair. These results contribute to our general understanding of SMUG1 activity under conditions it may encounter in the cell such as dynamic chromatin at pockets of liquid-liquid phase separation [7,8] and compartments of the nucleus [61]. Chromatin dynamics are largely influenced by ionic strength [10,12,16,21]. Furthermore, recent work demonstrated that salt-dependent changes in chromatin structure can modulate glycosylase activity. Using an oligo-nucleosome array containing 12 601 NCPs each separated by 30 bp of linker DNA, glycosylase activity was shown to be controlled by Mg^{2+} [73]. At 0.2 mM Mg^{2+}, the arrays adopt an extended "beads-on-a-string" conformation representing an open or accessible state of chromatin. At higher ionic strength of 2 mM Mg^{2+}, the arrays resemble compact and condensed chromatin fibers observed *in vivo* [73,74]. The rate of combined uracil DNA glycosylase (UDG) and AP endonuclease 1 (APE1) activity at a U OUT site is reduced ~3-fold on the compact array relative to the extended array (and ~20-fold relative to duplex DNA) [73]. Furthermore, at the higher ionic strength, UDG/APE1 activity is ~14-fold faster at this same site on arrays constructed using H4 histone lacking the N-terminal tail. This tail is known to mediate chromatin compaction via interactions with H2A on an adjacent nucleosome and increased repair activity in the absence of the tail is consistent with a more extended chromatin structure. Interestingly, at a U site in a linker region of the compacted

nucleosome array, UDG/APE1 activity is increased by 5-fold compared to duplex DNA. In other work, thymine DNA glycosylase (TDG) was unable to excise an OUT 5-formylcytosine from the histone-bound region of an array regardless of the level of compaction, although activity was observed in the linker region of extended, but not compact, arrays [11]. These results collectively support the conclusion that ionic strength and chromatin structure influence these BER enzymes.

SMUG1 has been generally postulated to be a backup glycosylase to other UDG superfamily members [42,43]. SMUG1 is constitutively expressed at low levels whereas expression of other superfamily members UDG and TDG is regulated during the cell cycle. UDG is upregulated during S-phase [43] and TDG is degraded at the G1-S boundary [75,76]. SMUG1 has a wide substrate specificity [77] and, unlike UDG and TDG, is present in the nucleolus [42]. In the eukaryotic cell, the nucleolus is responsible for ribosome biogenesis, where SMUG1 may encounter periods of more loosely packaged chromatin during the critical transcription of ribosomal DNA (rDNA) [78]. SMUG1 has also been shown to have a role in RNA processing [79], which may be beneficial in maintaining genomic integrity in the nucleolus. While the absolute concentrations of monovalent cations in the nucleousare unknown [61], our model system provides a snapshot of how nucleosome dynamics, in the context of repair, may be impacted by microenvironments of the cell nucleus. Our experimental conditions represent times of more and less compact nucleosomes in HIGH and LOW conditions respectively. Our results demonstrate SMUG1 is more efficient in low ionic strength, representative of when it may encounter damage in a less compacted nucleosome [10,12,17,22]. Rather than being a backup for other glycosylases, SMUG1 may serve particular roles as an important player in the maintenance of dynamic chromatin.

Broadly, SMUG1 excises U from NCP substrates more effectively in LOW conditions than HIGH. Considering that in duplex SMUG1 is unaffected by the changing ionic environment except at short incubation times, we hypothesize that most observed changes in SMUG1 activity at 60 min are due to NCP structure and dynamics. Notably, footprinting experiments reveal that each nucleobase in an NCP experiences a unique and nuanced microenvironments that may affect its accessibility to SMUG1 and other DNA processing enzymes. While considering the effects of ionic strength of the cellular environment on glycosylase activity, it is important to recognize that other cellular machinery and factors such as chromatin remodelers, histone PTMs, histone variants, and proteolytic clipping of histone tails may contribute to DNA accessibility [80-83]. The results obtained here describing SMUG1 excision of U from an NCP model system contribute to our understanding of BER and genomic integrity.

CRediT authorship contribution statement

Conceptualization, K.L.R., S.D.; Investigation, K.L.R.; Formal analysis, K.L.R.; Writing – Original Draft and Review & Editing, K.L.R., S.D.; Supervision, S.D.

Acknowledgments

This research was supported by the National Science Foundation (MCB-2111680). K.L.R. was supported by a National Institute of Environmental Health Sciences training grant (T32ES007272). We thank all the members of the Delaney laboratory for discussion and T. Sutton, J. Cook, and C. Jacques for critical reading of the manuscript.

Conflict of interest statement

The authors declare that there are no conflicts of interest.

Appendix A. Supporting information

Supplementary data associated with this article can be found in the online version.

References

[1] Warshel, A.; Russell, S. T. Calculations of electrostatic interactions in biological systems and in solutions. *Q. Rev. Biophys*. **1984**, *17*, 283-422.

[2] Honig, B.; Nicholls, A. Classical electrostatics in biology and chemistry. *Science* **1995**, *268*, 1144-1149. [3] König, I.; Zarrine-Afsar, A.; Aznauryan, M.; Soranno, A.; Wunderlich, B.; Dingfelder, F.; Stüber, J. C.; Plückthun, A.; Nettels, D.; Schuler, B. Single-molecule spectroscopy of protein conformational dynamics in live eukaryotic cells. *Nature Methods* **2015**, *12*, 773-779.

[4] Nørby, J. G.; Esmann, M. The effect of ionic strength and specific anions on substrate binding and hydrolytic activities of Na,K-ATPase. *J Gen Physiol* **1997**, *109*, 555-570.

[5] Marek, P. J.; Patsalo, V.; Green, D. F.; Raleigh, D. P. Ionic strength effects on amyloid formation by amylin are a complicated interplay among Debye screening, ion selectivity, and Hofmeister effects. *Biochemistry* **2012**, *51*, 8478-8490.

[6] Record, M. T.; Anderson, C. F.; Lohman, T. M. Thermodynamic analysis of ion effects on the binding and conformational equilibria of proteins and nucleic acids: the roles of ion association or release, screening, and ion effects on water activity. *Q. Rev. Biophys.* **1978**, *11*, 103-178.

[7] Sawyer, I. A.; Bartek, J.; Dundr, M. Phase separated microenvironments inside the cell nucleus are linked to disease and regulate epigenetic state, transcription and RNA processing. *Semin. Cell Dev. Biol.* **2019,** *90*, 94-103.

[8] Lafontaine, D. L. J.; Riback, J. A.; Bascetin, R.; Brangwynne, C. P. The nucleolus as a multiphase liquid condensate. *Nat. Rev. Mol. Cell Biol.* **2021,** *22*, 165-182.

[9] Czarnota, G. J.; Ottensmeyer, F. P. Structural states of the nucleosome. *J. Biol. Chem.* **1996,** *271*, 3677-83.

[10] Eltsov, M.; Grewe, D.; Lemercier, N.; Frangakis, A.; Livolant, F.; Leforestier, A. Nucleosome conformational variability in solution and in interphase nuclei evidenced by cryo-electron microscopy of vitreous sections. *Nucleic Acids Res.* **2018,** *46*, 9189-9200.

[11] Deckard, C. E.; Banerjee, D. R.; Sczepanski, J. T. Chromatin Structure and the Pioneering Transcription Factor FOXA1 Regulate TDG-Mediated Removal of 5-Formylcytosine from DNA. *J. Am. Chem. Soc.* **2019,** *141*, 14110-14114.

[12] Mozziconacci, J.; Victor, J.-M. Nucleosome gaping supports a functional structure for the 30 nm chromatin fiber. *J. Struct. Biol.* **2003,** *143*, 72-76.

[13] Luger, K.; Mäder, A. W.; Richmond, R. K.; Sargent, D. F.; Richmond, T. J. Crystal structure of the nucleosome core particle at 2.8 Å resolution. *Nature* **1997,** *389*, 251.

[14] Hazan N. P.; Tomov, T. E.; Tsukanov, R.; Liber, M.; Berger, Y.; Masoud, R.; Toth, K.; Langowski, J.; Nir, E. Nucleosome Core Particle Dissasembly and Assembly Kinetics Studied Using Single-Molecule Fluorescence. *Biophys. J.* **2015,** *109,* 1676-1685.

[15] Ruiz-Carrillo, A.; Jorcano, J. L.; Eder, G.; Lurz, R. In vitro core particle and nucleosome assembly at physiological ionic strength. *Proc. Natl. Acad. Sci. USA* **1979,** *76,* 3284-3288.

[16] Kim, J.; Wei, S.; Lee, J.; Yue, H.; Lee, T.-H. Single-Molecule Observation Reveals Spontaneous Protein Dynamics in the Nucleosome. *J. Phys. Chem. B* **2016,** *120*, 8925-8931.

[17] Ngo, T. T. M.; Ha, T. Nucleosomes undergo slow spontaneous gaping. *Nucleic Acids Res.* **2015,** *43*, 3964-3971.
[18] Davis, W. B.; Bjorklund, C. C.; Deline, M. Probing the effects of DNA-protein interactions on DNA hole transport: the N-terminal histone tails modulate the distribution of oxidative damage and chemical lesions in the nucleosome core particle. *Biochemistry* **2012,** *51*, 3129-42.
[19] Ren, M.; Greenberg, M. M.; Zhou, C. Participation of Histones in DNA Damage and Repair within Nucleosome Core Particles: Mechanism and Applications. *Acc. Chem. Res.* **2022**, *55*, 1059-1073.
[20] Fu, I.; Cai, Y.; Geacintov, N. E.; Zhang, Y.; Broyde, S. Nucleosome Histone Tail Conformation and Dynamics: Impacts of Lysine Acetylation and a Nearby Minor Groove Benzo[a]pyrene-Derived Lesion. *Biochemistry* **2017,** *56*, 1963-1973.
[21] Zhou, K.; Gaullier, G.; Luger, K. Nucleosome structure and dynamics are coming of age. *Nat. Struct. Mol. Biol.* **2019,** *26*, 3-13.
[22] Zlatanova, J.; Bishop, T. C.; Victor, J.-M.; Jackson, V.; van Holde, K. The Nucleosome Family: Dynamic and Growing. *Structure* **2009,** *17*, 160-171.
[23] Yang, K.; Prasse, C.; Greenberg, M. M. Effect of Histone Lysine Methylation on DNA Lesion Reactivity in Nucleosome Core Particles. *Chem. Res. Toxicol.* **2019,** *32*, 910-916.
[24] Kennedy, E. E.; Li, C.; Delaney, S. Global Repair Profile of Human Alkyladenine DNA Glycosylase on Nucleosomes Reveals DNA Packaging Effects. *ACS Chem. Biol.* **2019,** *14*, 1687-1692.
[25] Bilotti, K.; Tarantino, M. E.; Delaney, S. Human Oxoguanine Glycosylase 1 Removes Solution Accessible 8-Oxo-7,8-dihydroguanine Lesions from Globally Substituted Nucleosomes Except in the Dyad Region. *Biochemistry* **2018,** *57*, 1436-1439.
[26] Olmon, E. D.; Delaney, S. Differential Ability of Five DNA Glycosylases to Recognize and Repair Damage on Nucleosomal DNA. *ACS Chem. Biol.* **2017,** *12*, 692-701.
[27] Hinz, J. M.; Rodriguez, Y.; Smerdon, M. J. Rotational dynamics of DNA on the nucleosome surface markedly impact accessibility to a DNA repair enzyme. *Proc. Natl. Acad. Sci.* **2010,** *107*, 4646.
[28] Cole, H. A.; Tabor-Godwin, J. M.; Hayes, J. J. Uracil DNA Glycosylase Activity on Nucleosomal DNA Depends on Rotational Orientation of Targets. *J. Biol. Chem.* **2010,** *285*, 2876-2885.
[29] Beard, B. C.; Wilson, S. H.; Smerdon, M. J. Suppressed catalytic activity of base excision repair enzymes on rotationally positioned uracil in nucleosomes. *Proc. Natl. Acad. Sci.* **2003,** *100*, 7465-7470.
[30] Rodriguez, Y.; Smerdon, M. J. The structural location of DNA lesions in nucleosome core particles determines accessibility by base excision repair enzymes. *J. Biol. Chem.* **2013,** *288*, 13863-13875.
[31] Prasad, A.; Wallace Susan, S.; Pederson David, S. Initiation of Base Excision Repair of Oxidative Lesions in Nucleosomes by the Human, Bifunctional DNA Glycosylase NTH1. *Mol. Cell Biol.* **2007,** *27*, 8442-8453.
[32] Caffrey, P.; Kher, R.; Bian, K.; Li, D.; Delaney, S. Comparison of the Base Excision and Direct Reversal Repair Pathways for Correcting 1,N6-Ethenoadenine in Strongly Positioned Nucleosome Core Particles. *Chem. Res. Toxicol.* **2020**, *33,* 1888-1896.
[33] Caffrey, P. J.; Delaney, S. Nucleosome Core Particles Lacking H2B or H3 Tails Are Altered Structurally and Have Differential Base Excision Repair Fingerprints. *Biochemistry* **2021,** *60*, 210-218.

[34] Bilotti, K.; Kennedy, E. E.; Li, C.; Delaney, S. Human OGG1 activity in nucleosomes is facilitated by transient unwrapping of DNA and is influenced by the local histone environment. *DNA Repair (Amst)* **2017,** *59*, 1-8.
[35] Maher, R. L.; Wallace, S. S.; Pederson, D. S. The lyase activity of bifunctional DNA glycosylases and the 3′-diesterase activity of APE1 contribute to the repair of oxidized bases in nucleosomes. *Nucleic Acids Res.* **2019,** *47*, 2922-2931.
[36] Odell, I. D.; Newick, K.; Heintz, N. H.; Wallace, S. S.; Pederson, D. S. Non-specific DNA binding interferes with the efficient excision of oxidative lesions from chromatin by the human DNA glycosylase, NEIL1. *DNA Repair (Amst)* **2010,** *9*, 134-143.
[37] Ye, Y.; Stahley, M. R.; Xu, J.; Friedman, J. I.; Sun, Y.; McKnight, J. N.; Gray, J. J.; Bowman, G. D.; Stivers, J. T. Enzymatic excision of uracil residues in nucleosomes depends on the local DNA structure and dynamics. *Biochemistry.* **2012,** *30,* 6028-6038.
[38] Chua, E. Y. D.; Vasudevan, D.; Davey, G. E.; Wu, B.; Davey, C. A. The mechanics behind DNA sequence-dependent properties of the nucleosome. *Nucleic Acids Res.* **2012,** *40*, 6338-6352.
[39] Li, C.; Delaney, S. Histone H2A Variants Enhance the Initiation of Base Excision Repair in Nucleosomes. *ACS Chem. Biol.* **2019,** *14*, 1041-1050.
[40] Mao, P.; Brown, A. J.; Malc, E. P.; Mieczkowski, P. A.; Smerdon, M. J.; Roberts, S. A.; Wyrick, J. J. Genome-wide maps of alkylation damage, repair, and mutagenesis in yeast reveal mechanisms of mutational heterogeneity. *Genome Res.* **2017,** *27*, 1674-1684.
[41] Kemmerich, K.; Dingler, F. A.; Rada, C.; Neuberger, M. S. Germline ablation of SMUG1 DNA glycosylase causes loss of 5-hydroxymethyluracil- and UNG-backup uracil-excision activities and increases cancer predisposition of Ung−/−Msh2−/− mice. *Nucleic Acids Res.* **2012,** *40*, 6016-6025.
[42] Raja, S.; Van Houten, B. The Multiple Cellular Roles of SMUG1 in Genome Maintenance and Cancer. *Int. J. Mol. Sci.* **2021,** *22*, 1981.
[43] Kavli, B.; Sundheim, O.; Akbari, M.; Otterlei, M.; Nilsen, H.; Skorpen, F.; Aas, P. A.; Hagen, L.; Krokan, H. E.; Slupphaug, G. hUNG2 Is the Major Repair Enzyme for Removal of Uracil from U:A Matches, U:G Mismatches, and U in Single-stranded DNA, with hSMUG1 as a Broad Specificity Backup*. *J. Biol. Chem.* **2002,** *277*, 39926-39936.
[44] Wibley, J. E. A.; Waters, T. R.; Haushalter, K.; Verdine, G. L.; Pearl, L. H. Structure and Specificity of the Vertebrate Anti-Mutator Uracil-DNA Glycosylase SMUG1. *Mol. Cell* **2003,** *11*, 1647-1659.
[45] Tarantino, M. E.; Dow, B. J.; Drohat, A. C.; Delaney, S. Nucleosomes and the three glycosylases: High, medium, and low levels of excision by the uracil DNA glycosylase superfamily. *DNA Repair (Amst)* **2018,** *72*, 56-63.
[46] Li, C.; Rioux, K. L.; Delaney, S. Histone variants H3.3 and H2A.Z/H3.3 facilitate excision of uracil from nucleosome core particles. *DNA Repair (Amst)* **2022,** *116*, 103355.
[47] Nilsen, H.; Lindahl, T.; Verreault, A. DNA base excision repair of uracil residues in reconstituted nucleosome core particles. *EMBO J.* **2002,** *21*, 5943.
[48] Schmidt-Nielsen, B. Comparative physiology of cellular ion and volume regulation. *J. Exp. Zool.* **1975,** *194*, 207-219.
[49] Aplin, C. P.; Miller, R. C.; Kay, T. M.; Heikal, A. A.; Boersma, A. J.; Sheets, E. D. Fluorescence depolarization dynamics of ionic strength sensors using time-resolved anisotropy. *Biophys. J.* **2021,** *120*, 1417-1430.

[50] Palmer, L. G.; Civan, M. M. Distribution of Na+, K+ and Cl- between nucleus and cytoplasm in Chironomus salivary gland cells. *J Membr Biol* **1977,** *33*, 41-61.
[51] Dick, D. A. The distribution of sodium, potassium and chloride in the nucleus and cytoplasm of Bufo bufo oocytes measured by electron microbe analysis. *J. Physiol.* **1978,** *284,* 37-53.
[52] Pietrzyk, C.; Heinz, E. The sequestration of Na+, K+ and Cl- in the cellular nucleus and its energetic consequences for the gradient hypothesis of amino acid transport in Ehrlich cells. *Biochim. Biophys. Acta Biomembr.* **1974**, *352,* 397-411.
[53] Liu, B.; Poolman, B.; Boersma, A. J. Ionic Strength Sensing in Living Cells. *ACS Chem. Biol.* **2017,** *12*, 2510-2514.
[54] Vasudevan, D.; Chua, E. Y. D.; Davey, C. A. Crystal Structures of Nucleosome Core Particles Containing the '601' Strong Positioning Sequence. *J. Mol. Biol.* **2010,** *403*, 1-10.
[55] Luger, K.; Rechsteiner, T. J.; Richmond, T. J. Expression and Purification of Recombinant Histones and Nucleosome Reconstitution. *Chromatin Protocols* **1999**, *119*, 1-16.
[56] Luger, K.; Rechsteiner, T. J.; Richmond, T. J. Preparation of nucleosome core particle from recombinant histones. *Meth. Enzymol.* **1999**, *304*, 3-19.
[57] Jain, S. S.; Tullius, T. D. Footprinting protein–DNA complexes using the hydroxyl radical. *Nat. Protoc.* **2008,** *3*, 1092.
[58] Hayes, J. J.; Tullius, T. D.; Wolffe, A. P. The structure of DNA in a nucleosome. *Proc. Natl. Acad. Sci.* **1990,** *87*, 7405-7409.
[59] Das, R.; Laederach, A.; Pearlman, S. M.; Herschlag, D.; Altman, R. B. SAFA: semi-automated footprinting analysis software for high-throughput quantification of nucleic acid footprinting experiments. *RNA* **2005,** *11*, 344-354.
[60] Lowary, P. T.; Widom, J. New DNA sequence rules for high affinity binding to histone octamer and sequence-directed nucleosome positioning. *J. Mol. Biol.* **1998,** *276*, 19-42.
[61] Németh, A.; Längst, G. Genome organization in and around the nucleolus. *Trends Genet.* **2011,** *27*, 149-156.
[62] Satchwell, S. C.; Drew, H. R.; Travers, A. A. Sequence periodicities in chicken nucleosome core DNA. *J. Mol. Biol.* **1986,** *191*, 659-675.
[63] Buning, R.; van Noort, J. Single-pair FRET experiments on nucleosome conformational dynamics. *Biochimie* **2010,** *92*, 1729-1740.
[64] Lee, J. Y.; Lee, J.; Yue, H.; Lee, T.-H. Dynamics of nucleosome assembly and effects of DNA methylation. *J. Biol. Chem.* **2015,** *290*, 4291-4303.
[65] Doseth, B.; Ekre, C.; Slupphaug, G.; Krokan, H. E.; Kavli, B. Strikingly different properties of uracil-DNA glycosylases UNG2 and SMUG1 may explain divergent roles in processing of genomic uracil. *DNA Repair (Amst)* **2012,** *11*, 587-593.
[66] Cravens, S. L.; Stivers, J. T. Comparative effects of ions, molecular crowding, and bulk DNA on the damage search mechanisms of hOGG1 and hUNG. *Biochemistry.* **2016,** *55*, 5230-5242.
[67] Taylor, E. L.; Kesavan, P. M.; Wolfe, A. E.; O'Brien, P. J. Distinguishing specific and nonspecific complexes of alkyladenine DNA glycosylase. *Biochemistry.* **2018,** *57,* 4440-4454.
[68] Howard, M. J.; Wilson, S. H. DNA scanning by base excision repair enzymes and implications for pathway coordination. *DNA Repair (Amst)* **2018,** *71,* 101-107.
[69] Zhang, Y.; O'Brien, P. J. Repair of alkylation damage in eukaryotic chromatin depends on searching ability of alkyladenine DNA glycosylase. *ACS Chem. Biol.* **2015,** *11,* 2606-2615.

[70] Ngo, T. T.; Zhang, Q.; Zhou, R.; Yodh, J. G.; Ha, T. Asymmetric unwrapping of nucleosomes under tension directed by DNA local flexibility. *Cell* **2015,** *160*, 1135-44.
[71] Bashkin, J.; Hayes, J. J.; Tullius, T. D.; Wolffe, A. P. Structure of DNA in a nucleosome core at high salt concentration and at high temperature. *Biochemistry* **1993,** *32*, 1895-1898.
[72] Huang, Z.; Fasco, M. J.; Kaminsky, L. S. Optimization of Dnase I removal of contaminating DNA from RNA for use in quantitative RNA-PCR. *Biotechniques* **1996,** *20*, 1012-4, 1016, 1018-20.
[73] Banerjee, D. R.; Deckard, C. E.; Elinski, M. B.; Buzbee, M. L.; Wang, W. W.; Batteas, J. D.; Sczepanski, J. T. Plug-and-Play Approach for Preparing Chromatin Containing Site-Specific DNA Modifications: The Influence of Chromatin Structure on Base Excision Repair. *J. Am. Chem. Soc.* **2018,** *140*, 8260-8267.
[74] Song, F.; Chen, P.; Sun, D.; Wang, M.; Dong, L.; Liang, D.; Xu, R. M.; Zhu, P.; Li, G. Cryo-EM study of the chromatin fiber reveals a double helix twisted by tetranucleosomal units. *Science* **2014,** *344*, 376-80.
[75] Shibata, E.; Dar, A.; Dutta, A. CRL4Cdt2 E3 Ubiquitin Ligase and Proliferating Cell Nuclear Antigen (PCNA) Cooperate to Degrade Thymine DNA Glycosylase in S Phase*. *J. Biol. Chem.* **2014,** *289*, 23056-23064.
[76] Slenn, T. J.; Morris, B.; Havens, C. G.; Freeman, R. M.; Takahashi, T. S.; Walter, J. C. Thymine DNA Glycosylase Is a CRL4Cdt2 Substrate*. *J. Biol. Chem.* **2014,** *289*, 23043-23055.
[77] Pettersen, H. S.; Sundheim, O.; Gilljam, K. M.; Slupphaug, G.; Krokan, H. E.; Kavli, B. Uracil-DNA glycosylases SMUG1 and UNG2 coordinate the initial steps of base excision repair by distinct mechanisms. *Nucleic Acids Res.* **2007,** *35*, 3879-3892.
[78] Dubois, M.-L.; Boisvert, F.-M. The Nucleolus: Structure and Function. *The Functional Nucleus*, **2016**, 29-49.
[79] Jobert, L.; Skjeldam, H. K.; Dalhus, B.; Galashevskaya, A.; Vågbø, C. B.; Bjørås, M.; Nilsen, H. The human base excision repair enzyme SMUG1 directly interacts with DKC1 and contributes to RNA quality control. *Mol. Cell* **2013,** *49*, 339-345.
[80] Polo, S. E.; Almouzni, G. Chromatin dynamics after DNA damage: The legacy of the access-repair-restore model. *DNA Repair (Amst)* **2015,** *36*, 114-121.
[81] Yang, K.; Park, D.; Tretyakova, N. Y.; Greenberg, M. M. Histone tails decrease N7-methyl-2′-deoxyguanosine depurination and yield DNA–protein cross-links in nucleosome core particles and cells. *Proc. Natl. Acad. Sci.* **2018,** *115*, E11212-E11220.
[82] Ren, M.; Shang, M.; Wang, H.; Xi, Z.; Zhou, C. Histones participate in base excision repair of 8-oxodGuo by transiently cross-linking with active repair intermediates in nucleosome core particles. *Nucleic Acids Res.* **2021,** *49*, 257-268.
[83] Fu, I.; Geacintov, N. E.; Broyde, S. Molecular dynamics simulations reveal how H3K56 acetylation impacts nucleosome structure to promote DNA exposure for lesion sensing. *DNA Repair (Amst)* **2021,** *107*, 103201.